Exciton Interactions, Excimer Formation, and [2π+2π] Photodimerization in Nonconjugated Curcuminoid-BF 2 Dimers

Manon Catherin, Olatz Uranga-Barandiaran, Arnaud Brosseau, Rémi Métivier, Gabriel Canard, Anthony d'Aléo, David Casanova, Frederic Castet, Elena Zaborova, Frédéric Fages

Exciton Interactions, Excimer Formation and [2π+2π] Photodimerization in Nonconjugated Curcuminoid-BF_2 Dimers

Manon Catherin,[a] Olatz Uranga-Barandiaran,[b,c,d] Arnaud Brosseau,[e] Rémi Métivier,[e] Gabriel Canard,[a] Anthony D'Aléo,[a] David Casanova,*[b] Frédéric Castet,*[d] Elena Zaborova,*[a] and Frédéric Fages*[a]

[a] *M. Catherin, Dr. G. Canard, Dr. A. D'Aléo, Dr. E. Zaborova, Prof. F. Fages*
Aix Marseille Univ, CNRS, CINaM UMR 7325, Campus de Luminy, Case 913, 13288 Marseille (France)
E-mail: elena.zaborova@univ-amu.fr
frederic.fages@univ-amu.fr

[b] *O. Uranga-Barandiaran, Dr. D. Casanova*
Donostia International Physics Center (DIPC), Paseo Manuel de Lardizabal 4, 20018 Donostia, Euskadi (Spain)
E-mail: david.casanova@ehu.eus

[c] *O. Uranga-Barandiaran*
Kimika Fakultatea, Euskal Herriko Unibertsitatea (UPV/EHU), 20018 Donostia, Euskadi (Spain)

[d] *O. Uranga-Barandiaran, Prof. F. Castet*
Institut des Sciences Moléculaires (ISM, UMR CNRS 5255), University of Bordeaux, 351 Cours de la Libération, 33405 Talence (France)
E-mail: frederic.castet@u-bordeaux.fr

[e] *A. Brosseau, Dr. R. Métivier*
PPSM, ENS Paris Saclay, CNRS, Université Paris-Saclay, 94235Cachan (France)

Supporting information and the ORCID identification number(s) for the author(s) of this article can be found under:
https://

Abstract: We describe the synthesis of a series of covalently-linked dimers of quadrupolar curcuminoid-BF_2 dyes and the detailed investigation of their solvent-dependent spectroscopic and photophysical properties. In solvents of low polarity, intramolecular folding induces the formation of aggregated chromophores whose UV-Vis absorption spectra display the optical signature characteristic of weakly-coupled H-aggregates. The extent of folding and, in turn, of ground state aggregation is strongly dependent on the nature of the flexible linker. Steady-state and time-resolved fluorescence emission spectroscopies show that the Frenkel exciton relaxes into a fluorescent symmetrical excimer state with a long lifetime. Furthermore, our in-depth studies show that a weakly-emitting excimer lies on the pathway toward a photocyclomer. Two-dimensional ^{1}H NMR spectroscopy and Density Functional Theory (DFT) allowed establishing the structure of the photoproduct. To our knowledge, this represents the first example of a [2π+2π] photodimerization of the curcuminoid chromophore.

Introduction

The strong demand for advanced optoelectronic devices such as organic light emitting diodes and organic solar cells is leading to the generation of an ever-increasing number of new π-conjugated polymers and small molecules.[1] In all these devices the organization of the molecular components in the solid state largely determines the efficiency of collective phenomena such as charge carrier transport or exciton delocalization and, in turn, the device performance.[2] Understanding and *a fortiori* controlling finely the stacking of the chromophores is therefore a cornerstone towards the design of novel π-conjugated materials with cutting-edge photonic and electronic properties. Quadrupolar-like D-π-A-π-D (or A-π-D-π-A) chromophores where D and A are electron donating and accepting groups, respectively, are of great interest for applications in nonlinear optics, organic photonics and photovoltaics.[3] Ground state aggregation of quadrupolar molecules is increasingly investigated theoretically and experimentally.[4,5] Like many chromophores, quadrupolar dyes are excitonically coupled in the solid state and the spectral properties of their aggregates can be adequately described by the Frenkel exciton model.[4] However, because of their quadrupolar electronic structure, D-π-A-π-D dyes exhibit intriguing properties in the solid state emerging from the quadrupole-quadrupole interactions. The latter was shown to provide a route to nonconventional H-aggregates with a red-shifted absorption as a result of a non-Kasha behavior.[4c]

Deciphering the main intermolecular interactions that dictate spectroscopic and electronic properties of aggregated chromophores is a particularly difficult task. Moreover, predicting crystal arrangements in organic solids is elusive because molecular packing in small aggregates, single crystals and polycrystalline thin films is controlled by a manifold of intermolecular forces.[6] Designing bichromophoric molecules consisting of two dye units covalently linked by a flexible or rigid transparent spacer represents a chemical modeling approach to the assessment of stacking interaction and electronic coupling in model systems having a reduced number of degrees of freedom and a more or less controlled geometry.[7,8] Important insights into dye aggregation can be gained from the investigation of covalent dimers in diluted solutions, which is a further asset because conventional spectroscopic techniques can be used.[7-13] Excimer formation in flexible dimers of polycyclic aromatic hydrocarbons such as anthracene or pyrene has been the subject of intense research in the past.[9,10] These molecules display very weak, if any, ground state interaction, but can undergo excited state association leading to excimer emission. Excimer formation is a dynamic process involving a rapid change in geometry following photoexcitation and thus reflects the conformational behavior of the

flexible chain. On the other hand, ground state dimer structures can enable intramolecular exciton coupling and, in contrast to the excimerization driven dimer formation, their electronic absorption properties are profoundly affected.[7,12,13] While, many examples relate the investigation of ground state interaction in covalent dimers of dipolar dyes,[7d,f] the case of quadrupolar dyes has been scarcely envisaged.[13,14]

Over the last years, some of us have investigated the optical properties of boron difluoride complexes of curcuminoid dyes (curcuminoids-BF_2) in solution and in the solid state.[5,15] Curcuminoids-BF_2 have a quadrupolar-like structure with the central boron chelate acting as strong electron acceptor unit. Depending on the nature of the terminal electron donor groups, they display a broad range of optical and electronic properties in the solid state, such as near-infrared fluorescence emission,[5] thermally-assisted delayed fluorescence,[16] two-photon excited fluorescence,[17] amplified spontaneous emission,[16] and charge separation in bulk heterojunction organic solar cells.[18] Other groups also reported interesting photophysical and electronic properties of curcuminoids-BF_2,[19] including charge transport in nanojunctions[20] and enhanced photoacoustic responses.[21] Single-crystal X-ray diffraction studies have shown that curcuminoid backbones interact strongly in π-stacks.[5] The monochromophoric compound **R-Me** (Figure 1) provides a typical example of such tightly packed dye molecules in the crystal.[5] As a result, the absorption spectrum of a suspension of nanoparticles of **R-Me** in water has been shown to undergo a noticeably blue-shifted absorption maximum, reminiscent of a H-aggregate spectrum, along with the appearance of a red-shifted band (Figure S1 in the Supporting Information).[5] From a theoretical investigation using essential-state models (ESMs),[4b] Terenziani, Sissa et al. could evidence a H-type behavior in agreement with the experimental X-ray diffraction and spectroscopic results.

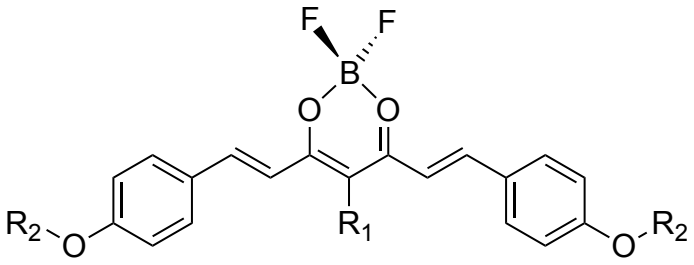

R_1	R_2	Compound
H	Methyl	**R-Me**
H	2-Ethylhexyl	**R-EH**
Ph	Methyl	**R-mPh-Me**

Figure 1. Structure of the monochromophoric dyes used as reference compounds in this study.

Recently, we reported the absorption spectra of two covalently-linked curcuminoid-BF_2 units, **C8-Me** and **C8-mPh-Me** (Figure 2), showing the H-type behavior of the intramolecularly aggregated dimer.[14] An in-depth theoretical study based on DFT and ESMs provided a characterization of the nature of the low-lying excited singlet states and converged to show the formation of H-aggregate species.[14] In this manuscript, we describe the synthesis of three new covalent dimers, **C12-Me**, **C12-EH** and **C6O2-Me** (Figure 2), and provide a detailed photophysical and photochemical investigation in solution. This series of compounds allowed us investigating the influence of the linker (chemical nature, length), and the effect of substitution at either the central carbon atom of the acetylacetonate unit (here called *meso* position R_1) or at the oxygen atoms of the terminal phenolic groups (R_2). From this study, we draw important conclusions on the fate of Frenkel excitons with regard to the solid-state behavior. Moreover, we describe the first case, to the best of our knowledge, of a [2π+2π] photodimerization involving the curcuminoid chromophore.

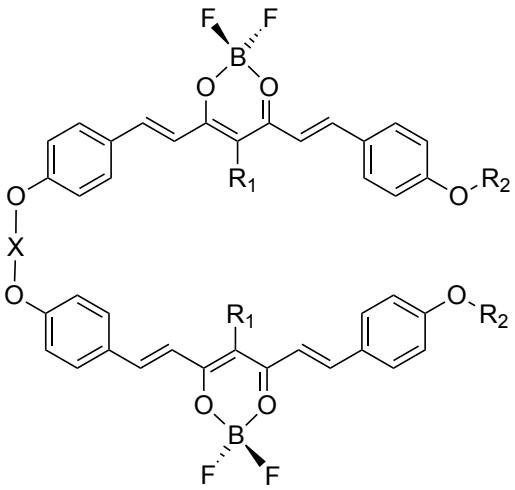

X	R_1	R_2	Compound
$-(CH_2)_8-$	H	Methyl	**C8-Me**
	Ph	Methyl	**C8-mPh-Me**
$-(CH_2)_{12}-$	H	Methyl	**C12-Me**
	H	2-Ethylhexyl	**C12-EH**
$-CH_2(CH_2OCH_2)_2CH_2-$	H	Methyl	**C6O2-Me**

Figure 2. Structure of the covalent dimers of curcuminoids-BF_2 investigated in this study.

Results

Synthesis and electrochemical properties

The synthesis of the covalent dimers involves the desymmetrization of the (acetylacetonato)difluoroboron moiety (Scheme 1) described previously for **C8-Me** and **C8-mPh-Me**.[14] The three new bis(curcuminoid-BF_2) compounds **C12-Me**, **C12-EH**, and **C6O2-Me** were prepared following the same procedures. The synthesis of the reference molecule **R-EH** and precursors to target compounds is described in the Supporting Information (Scheme

S1). The cyclic voltammograms (CVs) of the five compounds were recorded in DCM containing 0.1 M of $(n\text{-Bu})_4NPF_6$ and display two-electron irreversible oxidation and reduction waves consistent with the electrochemical properties of curcuminoids-BF_2 (Figure S2).[22] The oxidation and reduction half-wave potential values (Table S1) are very close to those obtained for the reference compounds, showing that tethering two curcuminoid-BF_2 units does not change significantly their electrochemical behavior in solution.

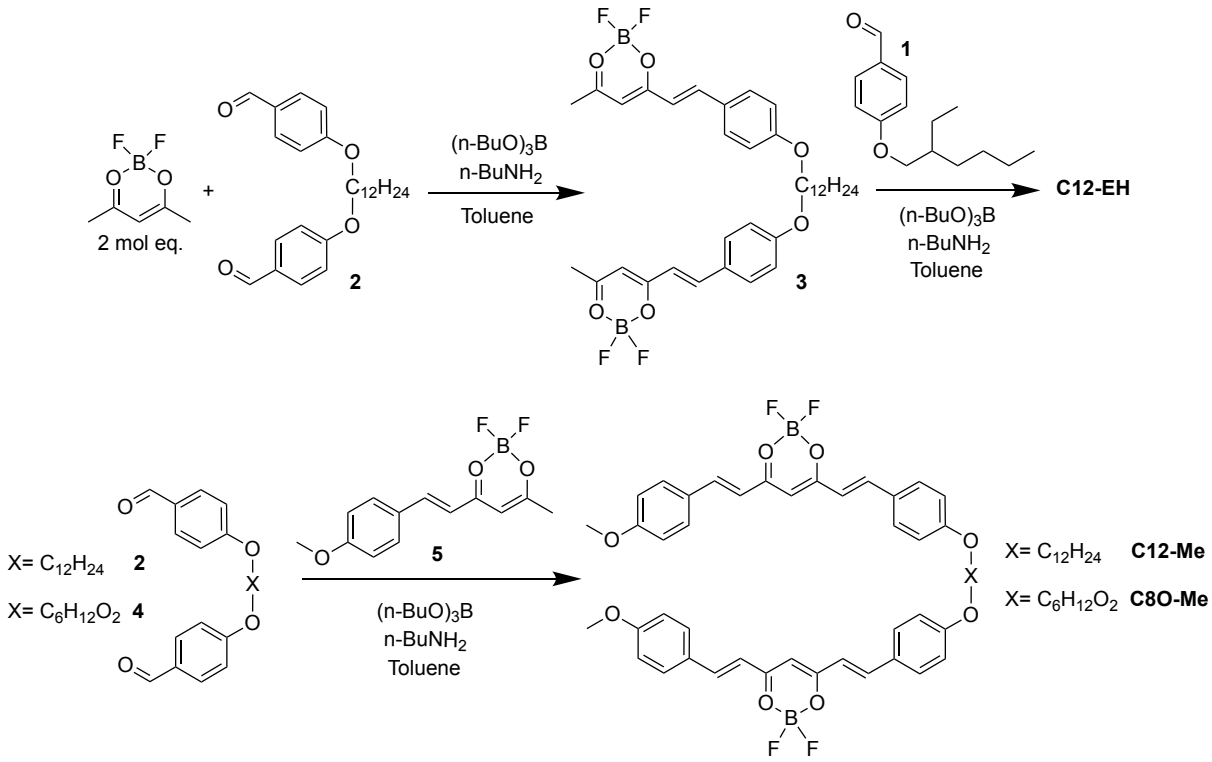

Scheme 1. Synthetic routes toward the bis(curcuminoid-BF_2) dimers.

Optical properties of the reference monochromophoric compounds

The steady-state absorption and fluorescence emission properties of **R-Me** and **R-mPh-Me** in diethyl ether (EE) and dichloromethane (DCM) as solvents were reported previously.[15] We recall here the main results for the sake of comparison with the bichromophoric compounds. The spectra show well-resolved vibronic structures and a mirror-image relationship in solvents of low polarity such as EE and di-*n*-butylether (BE) (Figures 3a and 4a). The optical features of the new reference compound **R-EH** (Figure 1) are identical to those of **R-Me** in BE, EE and DCM. Because branched alkyl chains provide a good solubility in alkanes, the spectra of **R-EH** could also be recorded in the apolar solvent cyclohexane (CH) (Figure S3). Owing to the charge transfer character of the ground and excited states of curcuminoid-BF_2 chromophores, absorption and fluorescence emission of curcuminoid-BF_2 dyes undergo significant spectral changes in solvents of different polarity. The spectra of **R-Me** and **R-mPh-Me** are broadened

and red shifted when passing from ether solvents (Stokes shift *ca*. 900-1100 cm^{-1}) to DCM (Stokes shift *ca*. 1700-2000 cm^{-1}). Moreover, the phenyl ring on the *meso* position of the curcuminoid backbone causes a bathochromic shift of *ca*. 15-17 nm of optical properties in all solvents investigated with respect to the unsubstituted chromophore **R-Me**. Fluorescence quantum yields Φ_f of **R-Me** and **R-mPh-Me** were reported previously and similar values (0.22 and 0.25, respectively) were obtained with BE as solvent.[15] Fluorescence emission spectra and Φ_f values of the reference dyes were found to be independent of the excitation wavelength and fluorescence excitation spectra matched the absorption profiles over the entire wavelength range. The fluorescence lifetimes in the three solvents are monoexponential in the subnanosecond to nanosecond regime. **R-Me** displays a short fluorescence lifetime (0.6 ns) in BE.

Steady-state spectroscopic properties of the bichromophoric compounds

The UV-Vis spectra of the bichromophoric compounds were investigated mainly in three solvents, BE, EE and DCM, and were concentration independent in the range of $5x10^{-7}$ - $5x10^{-8}$ M using cuvettes of 5 cm optical path. To begin, we detail the experimental results obtained with **C6O2-Me**. Like the reference compound **R-Me, C6O2-Me** shows a vibronic fine structure (Figure 3a), but the Franck-Condon progression undergoes a reversal in the 0-0 to 0-1 band absorbance ratio ($R_{abs} = A_{0\text{-}0}/A_{0\text{-}1} = 0.45$) with respect to that of **R-Me** ($A_{0\text{-}0}/A_{0\text{-}1} = 1.15$). As a result, the absorption maximum of **C6O2-Me** is blue shifted (λ_{max}^{abs} = 449 nm) compared to **R-Me** ($\lambda_{max}^{abs} = 475$ nm). At the low concentrations used, the absorbance and the shape of the spectrum did not show any significant variation when the solutions were incubated in the dark for more than 24 hours. Therefore, the change in optical properties stems from the electronic absorption of a ground state covalent dimer in which the two chromophores experience an intramolecular excitonic interaction. The term aggregate dimer is used hereafter to designate this species, while nonaggregated dimer will indicate non-interacting monomers in the dimer. Increasing the polarity of the solvent from BE and EE to DCM restores partly the profile of the vibronic progression ($R_{abs} = 0.93$) found in the absorption spectrum of the reference molecule **R-Me** (Figure S4). Adding DCM to a diluted BE solution of **C6O2-Me** also leads to an increase of the value of R_{abs} showing that aggregated and nonaggregated dimers interconvert in the ground state.

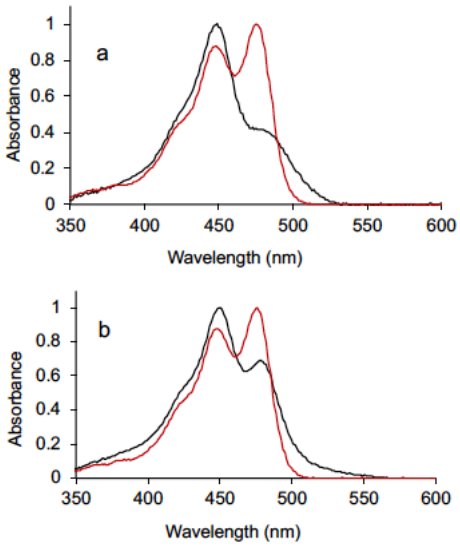

Figure 3. UV-Vis spectra of **R-Me** (red line) and of the bichromophoric compounds: a) **C6O2-Me** (black line) and b) **C8-Me** (black line). Concentration 5×10^{-7} – 10^{-6} M in BE. Spectra are normalized to unity at the absorption maximum.

In contrast to the case of **R-Me**, the fluorescence emission spectrum of **C6O2-Me** in BE displays two emission bands (Figure 4a). The one at high energy (λ_{max}^{em} = 498 nm) is structured and, except for a bathochromic shift of less than 5 nm, resembles that of the reference chromophore **R-Me**. This monomer-like emission can be attributed to the presence in BE of a population of nonaggregated dimers featuring unperturbed chromophores in the singlet excited state. The slight bathochromic shift can be related to the fact that the photoexcited chromophore in the bis(curcuminoid-BF_2) is subjected to the dipole field of the other one in the ground state and thus feels locally an increased polarity. A second emission is detected at low energy (λ_{max}^{em} > 600 nm) as a broad structureless emission band which resembles that of an excimer. The intensity of that emission increases at the expense of the monomer-like one when the excitation wavelength λ_{exc} is set at 440-450 nm where the absorption mostly arises from the aggregate. Conversely, the monomer-like emission more largely dominates upon excitation at λ_{exc} = 465-480 nm corresponding mainly to the absorption of the unperturbed chromophore (Figure 4a). Consistently, the shape of the fluorescence excitation spectra in BE depends strongly on the observation wavelength λ_{obs} (Figure 4b). The excitation spectrum of **C6O2-Me** monitored at λ_{obs} = 650 nm, that is at the red tail of the excimer-like emission spectrum, is very similar to that of the absorption spectrum, the value of the fluorescence intensity ratio $I_{0\text{-}0}/I_{0\text{-}1}$ = 0.41 being close to that of R_{abs}. This indicates that the aggregate is the major absorbing species in solution. When the emission is observed at λ_{obs} = 498 nm (Figure 4b), that is at the monomer-like band,

the ratio ($I_{0\text{-}0}/I_{0\text{-}1}$ = 0.90) in the excitation spectrum of **C6O2-Me** becomes closer to the R_{abs} value characteristic of **R-Me**. Because there is no significant spectral contribution of monomer-like emission at 650 nm, it can be inferred that the excimer species is related to the radiative relaxation of the Frenkel exciton in the aggregate. These observations indicate that the fraction of nonaggregated bis-curcuminoid molecules **C6O2-Me** in BE is very small and can hardly be detected in the UV-vis spectrum. However, owing to the higher Φ_f of the unperturbed photoexcited chromophores, their contribution becomes noticeable in the emission and excitation spectra. Moreover, we find the same dependence of emission and excitation profiles on excitation and observation wavelengths, respectively, in EE (Figure S5). In DCM, one observes the quasi disappearance of the excimer-like emission at the benefit of the monomer like-one, which is consistent with the absorption data (Figure S5).

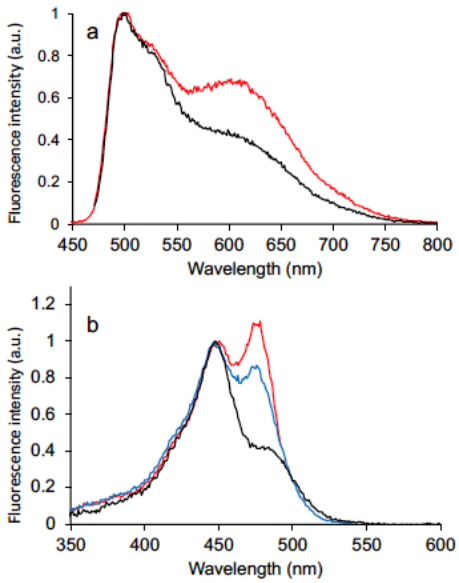

Figure 4. Steady-state fluorescence of **C6O2-Me**: a) fluorescence emission spectra recorded at λ_{exc} = 440 nm (red line) and 465 nm (black line) and normalized to unity at the emission maximum; b) excitation spectra recorded at λ_{obs} = 650 nm (black line), 550 nm (blue line) and 498 nm (red line) and normalized to unity at 449 nm. Concentration < 10^{-6} M in BE.

The overall fluorescence quantum yield Φ_f of **C6O2-Me** in BE obtained with λ_{exc} = 465 nm is very low (0.06) and is only slightly higher than that obtained at λ_{exc} = 440 nm (0.05). Assuming that Φ_f of unperturbed chromophores is close to that of **R-Me** (Φ_f = 0.44),[15] the low value of the overall fluorescence quantum yield further supports the assumption that the amount of nonaggregated dyes is small in BE. Φ_f determined in DCM increases substantially (0.27, λ_{exc}

= 465 nm), but does not reach the value of the reference chromophore (0.44), which confirms that aggregates are also present in DCM although to a lesser extent.

The steady-state spectroscopic properties of the two bichromophoric compounds, **C8-Me** and **C12-Me**, in BE, EE, and DCM are similar and show a decrease of the absorbance ratio $A_{0\text{-}0}/A_{0\text{-}1}$ as noticed for **C6O2-Me**. However, we note that the values of this ratio in the three solvents are systematically higher than those of **C6O2-Me** (Figure 3b). We found a value of *ca*. 0.73 in BE and 1.1 in DCM for both **C8-Me** and **C12-Me**. Unlike the case of **C6O2-Me** in BE, the excimer-like emission is very weak and the fluorescence spectra of **C8-Me** and **C12-Me** obtained at λ_{exc} = 440 nm and 465 nm are very similar (Figure 5a, Figure S6). Compared to **R-Me**, we only notice a longer emission tail at low energy. The shape of the fluorescence excitation spectra obtained in BE (Figure 5b) depends on the observation wavelength and reproduces well the corresponding absorption profiles when they are monitored at $\lambda_{obs} > 600$ nm. When λ_{obs} = 498 nm, the excitation spectrum of **C8-Me** and **C12-Me** in BE matches that of the reference compound **R-Me**. These observations specify a smaller amount of aggregates in BE when the two curcuminoid units in **C8-Me** and **C12-Me** are tethered by 8- and 12-membered α,ω-alkyl chains. Consistently, Φ_f values are higher than those obtained for **C6O2-Me**. However, despite the quasi absence of the excimer emission, the overall fluorescence efficiency remains lower than that of the monochromophoric compound **R-Me** (Φ_f = 0.09 - 0.14), which indicates the occurrence of an efficient quenching process in the excited state (*vide infra*). In DCM, Φ_f of **C8-Me** (0.42) and **C12-Me** (0.40) reaches the value characteristic of **R-Me** and this is in agreement with the absorption data, the spectra of three compounds having the same R_{abs} value in DCM.

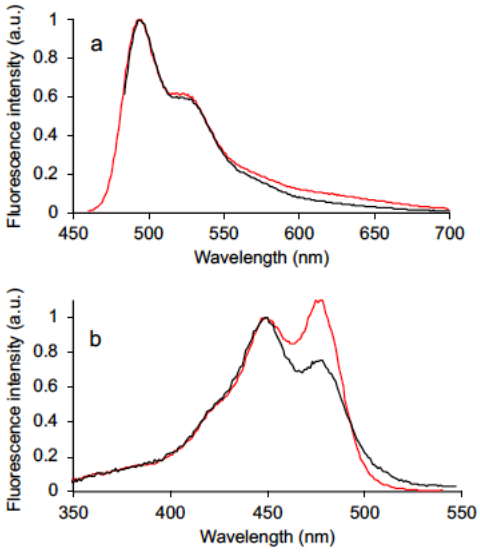

Figure 5. Steady-state fluorescence of **C8-Me**: a) fluorescence emission spectra obtained at λ_{exc} = 450 nm (red line) and 475 nm (black line) and normalized to unity at the emission maximum; b) excitation spectra obtained at λ_{obs} = 550 nm (red line) and 600 nm (black line) and normalized to unity at 449 nm. Concentration < 10^{-6} M in BE.

The ethylhexyl chain in **C12-EH** does not affect significantly the aggregation process in BE relative to **C12-Me** as evidenced from the identical $A_{0\text{-}0}/A_{0\text{-}1}$ absorbance ratio in this solvent (Table S2, Figure S6). Previously,[14] we showed that aggregate formation in **C8-mPh-Me** in BE is much less pronounced than for **C8-Me** and this can be ascribed to the bulk of the *meso*-phenyl ring. Interestingly, the change in chemical substitution leads to a significant increase of solubility of **C12-EH** and **C8-mPh-Me** in the apolar cyclohexane (CH) solvent. While the optical properties of **C8-mPh-Me** do not change drastically in CH relative to BE owing to the crowding of the curcuminoid backbone (Figure S7), compound **C12-EH** shows instead a marked propensity to generate the aggregated dimer in CH (Figure S3). Interestingly, its behavior in this solvent is comparable to that of **C6O2-Me** in BE. Indeed, a small value of $A_{0\text{-}0}/A_{0\text{-}1}$ (0.485) is determined from the absorption spectrum of **C12-EH** in CH and the intramolecular excimer-like fluorescence is rather intense. We also find a dependence of fluorescence emission and excitation spectra on excitation and emission wavelength, respectively, similar to that of **C6O2-Me** in BE.

Time-resolved fluorescence emission

Fluorescence emission decays of **C8-Me** and **C6O2-Me** in BE were recorded at four emission wavelengths extending from monomer- to excimer-like spectral domains. The same measurements were performed on **C12-EH** in CH at three emission wavelengths. Identical sets of decay time constants were obtained for two excitation wavelengths (440 and 480 nm). The decay curves were deconvoluted by a sum of four exponential terms, indicating the occurrence for all compounds of four kinetically distinguishable species in the excited state (Figure S8). All the decays were also analyzed by a global analysis procedure using a four-exponential fitting function, which allowed us to determine the decay time constants τ_i and the pre-exponential factors $a_i(\lambda)$ (i = 1-4). All fits were satisfactory with $\chi_R^2 < 1.2$. From the values of τ_i and $a_i(\lambda)$ at the four wavelengths investigated, we calculated the normalized fraction of intensity $f_i(\lambda)$ (Figures 6 and S9).[23] The data are collected in Table S3. Remarkably, they show very similar patterns for the three compounds. The species with τ_2 = 0.53–0.58 ns has a large value of $f_2(\lambda)$ at high energy and can be unambiguously attributed to the locally excited state of

the nonaggregated chromophore, which is consistent with the conclusions drawn from the steady-state measurements. The longest component τ_4 = 9 – 9.4 ns showing a strong value of $f_4(\lambda)$ that increases at longer emission wavelengths can be ascribed to the excimer-like emission. The $f_3(\lambda)$ value showing a maximum around 575 nm and associated to a long component (τ_3 = 1.6–2 ns) cannot be assigned to a locally-excited state. It rather stems from a second excimer species. Finally, the very short component τ_1 = 70–150 ps detected in the high energy part of the fluorescence spectrum, with a very small contribution (f_1 = 0.01–0.06), probably stems from a strongly quenched locally excited state. A rational interpretation of these results is given below in the discussion part.

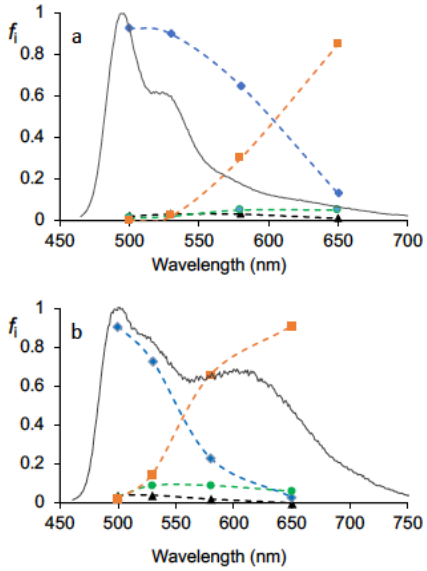

Figure 6. Four exponential decay analysis (λ_{exc} = 440 nm) of a) **C8-Me** and b) **C6O2-Me** showing the normalized fraction of intensity $f_i(\lambda)$ (i = 1 – 4) as a function of the emission wavelength λ calculated for each value of τ_i: τ_1 = 70 – 150 ps (black); τ_2 = 0.53 – 0.58 ns (blue); τ_3 = 1.6 – 2 ns (green); τ_4 = 9 – 9.4 ns (orange). The grey solid line represents the steady-state fluorescence emission spectra (λ_{exc} = 440 nm). Concentration < 10^{-6} M in BE.

Photochemical properties

We investigated the photochemical reactivity of the four compounds, **C6O2-Me**, **C8-Me**, **C12-Me** and **C12-EH**. Diluted solutions in EE (containing ca. 2 vol % of DCM to avoid precipitation) were exposed to visible light at room temperature using a flood lamp (Osram 100 W) in 1 cm pathway quartz cells for UV-Vis monitoring and 1 liter Pyrex flasks for preparative purposes. The UV-Vis spectral features of these solutions were identical to those described above (**C6O2-Me**: $A_{0\text{-}0}/A_{0\text{-}1}$ = 0.52; **C8-Me**: $A_{0\text{-}0}/A_{0\text{-}1}$ = 0.84; **C12-Me**: $A_{0\text{-}0}/A_{0\text{-}1}$ = 0.89; **C12-**

EH: $A_{0\text{-}0}/A_{0\text{-}1} = 0.91$) and the maximum absorbance of all the solutions was adjusted to the same value (0.18-0.20, conc. *ca*. 10^{-6} M) at the absorption maximum.

For all compounds, continuous irradiation induces a profound modification of the absorption spectrum with a decrease of the bis(curcuminoid-BF_2) absorbance along with the appearance of a new band at higher energy (Figures 7 and S10). The spectra obtained at the end of the reaction consist of a superimposition of the photoproduct and bichromophore absorptions. Due to that spectral overlap, it is likely that the reaction cannot reach completion while irradiation results in no further spectral changes. The variation of absorbance over irradiation time and the formation of sharp isosbestic points suggest that the photoreaction proceeds smoothly without formation of by-products, which indicates that the bichromophoric molecules convert into a single chemical species. Because bubbling argon into the solutions did not influence the course of the photoreaction, the participation of a triplet state can be excluded and the photoreaction thus takes place from the first singlet excited state.

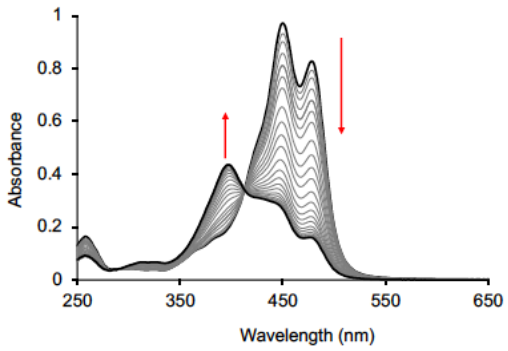

Figure 7. Changes in the UV-Vis spectrum of the EE solution of **C8-Me** upon irradiation with a continuous wave white light for different times. The final spectrum was obtained for an irradiation time of 1 hour. Concentration $5x10^{-6}$ M. The initial spectrum is normalized to unity at the absorption maximum.

Visible irradiation of **C8-Me**, **C6O2-Me** and **C12-EH** (5 mg in 500 mL EE) under preparative conditions leads to a mixture of the starting bichromophore and photoproduct. The photoproduct of all bichromophoric compounds was observed to be thermally unstable at room temperature, which necessitated to record NMR spectra just after evaporation to dryness of the reaction mixture. Therefore, no attempt was made to separate reactants and products and the ^{1}H NMR spectra of the reaction mixtures were recorded (Figures S11-S17, Scheme S2, Table S4). The aromatic part of the NMR spectra of the photoproducts reveal new resonance peaks in addition to the signals belonging to the unreacted molecule. They feature the AX pattern characteristic of the olefinic bond with the *E* configuration (J_{AX} = 16 Hz), but the integration

value amounts for a total of two protons *per* curcuminoid unit. This indicates that one curcuminoid C-C double bond is no longer present in the photoproduct while the other one is left unreacted, which is consistent with the UV-Vis spectrum of the photoproduct showing an absorption band at *ca*. 395 nm similar to that recorded for a hemicurcuminoid derivative.[24] The phenyl proton resonances are split, which further indicates desymmetrization of the curcuminoid backbone. Importantly, new resonance peaks are found at higher field at *ca*. 3.6 - 3.8 ppm which are characteristic of a cyclobutane structure.[25] These results show that the three compounds undergo a photocyclomerization *via* the intramolecular [2π+2π] photodimerization of two curcuminoid units forming two hemicurcuminoid fragments. From the symmetry of the cyclobutane AA'BB' spin system, it can be concluded that the photocyclomers have the *trans* configuration, which indicates that the reaction is stereospecific. 2D ROESY experiments (500 MHz, DMSO-d_6) indicate that the flexible link bridges the two hemicurcuminoid moieties. These features lead one to consider two possible photoproduct structures, A and B, in which the hemicurcuminoid halves experience a *trans* (A) or a *cis* (B) relationship with respect to the cyclobutane ring (Figure 8).

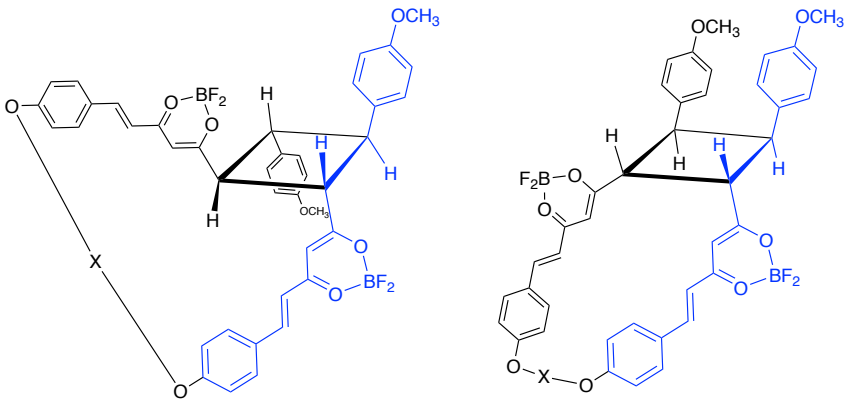

Figure 8. Structures of the photoproducts. Left: structure A; right: B.

DFT calculations at the ωB97XD/6-31+G(d) level provided the energy of the optimized geometry of structures A and B for the photoproducts **PC8-Me** and **PC6O2-Me** of **C8-Me** and **C6O2-Me**, respectively (Figure S18). For both compounds, the bridging chain is found to be long enough to enable the formation of structure A despite a quite large distance separating terminal phenolic oxygen atoms. In the case of **PC8-Me**, the -$(CH_2)_8$- chain of A adopts a fully extended all-*trans* conformation, which is the energetically favorable one for alkane chains. This may serve to balance the cost in energy induced by the stronger deviation from planarity of the cyclobutane ring in structure A with respect to B. The electronic energies of the two

structures are very similar with A being more stable than B by less than 1 kcal/mol for **PC8-Me** and by 1.5 kcal/mol for **PC6O2-Me**. It is well known that the degree of overlap of the two olefinic bonds is a critical parameter in the cyclic transition state, double bond parallelism being the most appropriate orientation for the photodimerization reaction to occur.[26] Simple geometrical considerations show that this condition implies that the transition state leading to B involves i) two curcuminoid units with their ground state dipole moments parallel, which is sterically too demanding and electrostatically unfavorable, or ii) a rotamer of one of the two curcuminoid chromophores resulting from a rotation around the single bond between the boron chelate and the olefinic bond during the exciton lifetime. Because these two possibilities seem very unlikely, we conclude that structure A is the most probable one.

Photochemical experiments using white light irradiation were performed several times for each compound. Under these conditions, we observed that the photoreaction of **C6O2-Me** takes a significantly longer time (*ca*. 2 hours) to achieve the same conversion relative to **C8-Me** and **C12-Me** (50 and 40 minutes, respectively). In order to get a more reliable evaluation of the relative photochemical efficiencies, we carried out irradiations of **C8-Me** and **C6O2-Me** in EE with excitation at two wavelengths, 449 nm and 478 nm, using a xenon lamp equipped with a monochromator. The irradiation time was adjusted so as to limit the decrease of absorbance to 15 - 20 % of the initial value. At this early stage of the photochemical transformation, the absorbance at the excitation wavelength of the photoproduct can be neglected. Irrespective of the excitation wavelength, these experiments further confirmed that the photoreaction in EE is slower for **C6O2-Me** than for **C8-Me** and **C12-Me**. It is worth noting that the weaker ground state intramolecular aggregation, the faster the photodimerization.

Discussion

The behavior of the bis(curcuminoid-BF_2) compounds in diluted solution can be rationalized by considering the occurrence of a solvent-polarity driven ground state equilibrium between unfolded and folded conformers.[7d] Because curcuminoids-BF_2 possess a strong ground state dipole moment, oriented perpendicularly to the molecular main axis, the interconversion between those sets of conformers is largely governed by dipole-dipole interactions. In apolar solvents, dipolar intramolecular interactions between chromophoric units provides the driving force toward intramolecular aggregation in the folded species. Conversely, in polar solvents, electrostatic interactions between dye moieties and dipolar solvent molecules dominate, which leads unfolded molecules to behave spectroscopically as monomer species. From UV-Vis absorption and fluorescence data, intramolecular pairing of the two chromophores is facilitated in the case of **C6O2-Me** compared to the other derivatives and the aggregate resulting from

chain folding represents by far the major species present in solution. It is known that the polyoxyethylene chain adopts a preferential helicoidal structure in solution and in the crystal because it can experience gauche conformations,[27] the oxygen atom lowering the rotational energy barrier of the C-C bond. This behavior contrasts with the conformational preference of the polymethylenic chain which is less prone to produce end-to-end cyclization because it is less flexible than the oxygen-containing counterpart.[11]

Irrespective of chain length and nature, the UV-Vis absorption spectra of the five compounds reveal the same excitonic feature characterized by a significant increase of the oscillator strength of the 0-1 vibronic band at the expense of the 0-0 and, as a result, a blue-shift of the absorption maximum. This specific spectral signature shows evidence of the formation of an intramolecular H-aggregate in which exciton interaction induces vibronic couplings.[28] Neglecting the contribution of the minor unfolded species, one can assume that the UV-Vis spectrum of **C6O2-Me** in BE provides the band profile of the pure H-aggregate. Under this assumption, the free-exciton band width W can be calculated from R_{abs} where $\bar{\nu}_0$ is the vibrational wavenumber:[28]

$$R_{\text{abs}} = \frac{A_{0-0}}{A_{0-1}} = \frac{(1 - 0.24\,W/\bar{\nu}_0)^2}{(1 + 0.073\,W/\bar{\nu}_0)^2}$$

This value has to be compared to the nuclear relaxation energy $\lambda^2\bar{\nu}_0$, where λ^2 is the Huang-Rhys factor. To obtain λ and $\bar{\nu}_0$, the vibronic progression in the absorption spectrum of **R-Me** in BE was analyzed according to:[29]

$$A(\bar{\nu}) = \sum_{v=0,1,2,\ldots} \frac{\lambda^{2v} e^{-\lambda^2}}{v!} \Gamma(\bar{\nu} - \bar{\nu}_{0-0} - v\bar{\nu}_0)$$

where $\bar{\nu}_{0-0}$ is the 0-0 transition wavenumber. Using the Gaussian line shape $\Gamma(\bar{\nu}) = \exp(-\bar{\nu}^2/\sigma^2)$, we obtain σ= 670 cm^{-1}, $\bar{\nu}_{0-0}$ = 21064 cm^{-1}, $\bar{\nu}_0$= 1321 cm^{-1} and λ^2 = 0.96 (Figure S19). Finally, using R_{abs} = 0.45, we obtain a value of 1500 cm^{-1} (186 meV) for W, which means $W \approx \lambda^2\bar{\nu}_0$ (1268 cm^{-1}). This confirms that excitonic coupling operates in the intermediate coupling regime leading to the typical distortion of the Franck-Condon progression observed in the experimental aggregate spectrum.[28]

The fluorescence emission spectra of **C6O2-Me**, **C8-Me**, **C12-Me** and **C12-EH** are obtained as the sum of two main contributions: a high energy band corresponding to the locally-excited state in unfolded bis(curcuminoid-BF_2) dimers and the low energy emission of excimer

states. Actually, fluorescence decays reveal the presence of two excimer species. The formation of two excimers with geometries differing by the relative orientation of the pyrene moieties has been commonly observed for 1,ω-bis(1-pyrenyl)alkanes.[30] In this case, a symmetrical pyrene excimer, characterized by a full overlap, is usually long-lived relative to the asymmetrical one. The initially formed Frenkel exciton in H-aggregated perylene bisimide assemblies has been shown to lose its coherence *via* ultrafast relaxation into an excimeric state.[31] Assuming that a similar process occurs in bis(curcuminoid-BF_2) compounds and according to the fact that theoretical data show that the two intramolecularly H-aggregated curcuminoids units form a sandwich-like structure,[14] we infer that the red-shifted (λ_{em} > 600 nm) long-lived (τ_4 = 9 – 9.4 ns) emission correlates with Frenkel exciton localization and formation of a symmetrical excimer E_{sym}. The second excimer, E_{asym}, having a weak emission and a shorter lifetime (τ_3 = 1.6 – 2 ns) compared to E_{sym} could be assigned to an asymmetrical structure characterized by an increase of the azimuth angle between π-systems long axes. As a result, this geometry would lead to a reduction of the torsion angle between the two olefinic double bonds located at the remote position from the tether in the molecular pair, that is a geometry close to that of the transition state of the photodimerization. As mentioned above and according to Schmidt's rule,[26] olefinic double bond parallelism is a prerequisite for the solid-state photodimerization reactions of cinnamic acid derivatives. Therefore, we can reasonably suggest that E_{asym} lies on the pathway toward the photoproduct. The question arises of how E_{asym} forms. Although the possibility that it results from a relaxation process of the Frenkel exciton competing with E_{sym} cannot be completely ruled out, this seems unlikely because exciton relaxation has been shown to occur on an ultrashort time scale leaving little chance for large amplitude geometrical changes to occur.[31] A more likely explanation is based on the occurrence of a bent conformation of bis(curcuminoid-BF_2) molecules having a ground state geometry intermediate between that of folded and unfolded species. The chromomophores in the bent dimer would experience no ground state intramolecular interaction in solution. Upon photoexcitation, the bent species would lead to a locally excited state having a very short lifetime (τ_1 = 70 – 150 ps) compared to the unfolded species (τ_2 = 0.53 – 0.58 ns), because it has the well-preorganized geometry to undergo an efficient relaxation toward E_{asym}. Accordingly, a short-time component τ_1 with a negative amplitude should be present to account for the dynamic formation of E_{asym}.[32] The fact that we did not observe any rise time in the fluorescence decays may be due to spectral overlap and probably to a small absolute value of the amplitude. This interpretation is consistent with the fact that **C8-Me** and **C12-Me** undergo a fast photoreaction if one considers that the

alkane tether i) is observed here to hinder folded H-aggregates leading preferentially to E_{sym} and ii) is generally known to be flexible enough to generate bent conformations enabling fast excimer and photoproduct formation.[10,11] These conclusions are summarized in a kinetic scheme that outlines the photophysics of the bis(curcuminoid-BF_2) molecules in BE solution (Scheme 2). While the unfolded-to-bent conformer excited state process can not be completely excluded from our results, the reverse reaction is less likely because of the very short excited state lifetime of the bent species. From the steady-state spectroscopic and time resolved fluorescence measurements, **C12-EH** containing a 12-membered chain behaves in CH like **C6O2-Me** in BE.

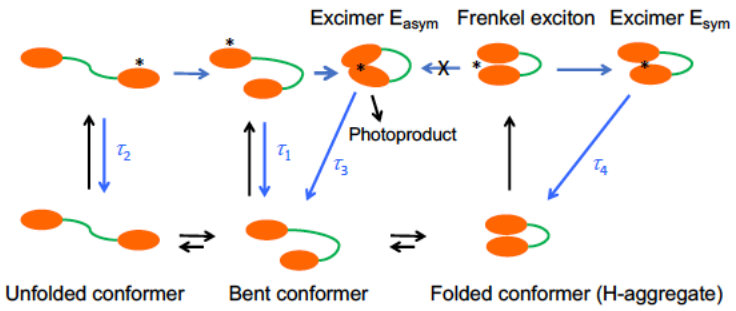

Scheme 2. Kinetic scheme for the covalent dimers of curcuminoids-BF_2 in solution.

Conclusion

A series of nonconjugated curcuminoid-BF_2 dimers was designed and synthesized in order to provide chemical models enabling the investigation of the photophysics, photochemistry and excited state processes in pairs of those quadrupolar chromophores. Steady-state optical and time-resolved fluorescence emission spectroscopies point to a similar behavior for the five nonconjugated dimers in the ground and excited states, those compounds being prone to ground state intramolecular H-aggregate formation in solvents of low polarity. This process is chain- and solvent-controlled and also depends on steric factors, such as the bulk imparted by the phenyl substituent on the *meso* position. The flexible polyoxyethylene chain in **C6O2-Me** favors a folded conformation leading almost exclusively to a H-aggregate in BE. The Frenkel exciton state then relaxes into a fluorescent symmetrical excimer state with a long lifetime. On the opposite, the stiffer polymethylenic chain in **C8-Me** and **C12-Me** leads preferentially to ground state extended and bent conformations whose fluorescence emission properties are characteristic of the reference chromophore. The formation of the asymmetric excimer with a shorter lifetime results from an excited state dynamic process involving those conformers featuring nonaggregated curcuminoid-BF_2 chromophores. **C6O2-Me**, **C8-Me** and

C12-Me undergo an intramolecular [2π+2π] photodimerization to give rise to the formation of a photocyclomer with the same structural features. Because the photocyclomer lies on the relaxation pathway of the asymmetric excimer, the photoreaction is faster for **C8-Me** and **C12-Me** compared to **C6O2-Me**, which reflects the ground state conformational preference of the different tethers. The solution study of curcuminoid-BF_2 quadrupolar chromophores tethered *via* a flexible nonconjugated linker provides not only a simple entry to the experimental correlation with their solid-state optical properties but also a new vision of their excited state behavior. Especially, this approach allows unveiling the first case of a [2π+2π] photodimerization of the curcuminoid backbone, a phenomenon that we have never observed in crystals nor concentrated solutions of **R-Me**. Interestingly, we reproduce here the H-aggregate exciton feature in the UV-vis absorption spectra that we reported previously for the crystalline assemblies of **R-Me**.[5] However, fluorescence emission in crystals of **R-Me** occurs at much lower energy relative to that of the excimer state in the nonconjugated dimers investigated in this study, which means that more reliable descriptors of the interaction between curcuminoid-BF_2 chromophores are still needed in order to reproduce finely the optical properties of these dyes in the solid state. In particular, previous computational studies[4b,14] revealed significant charge transfer contributions. Mixing between Frenkel and charge-transfer excitations is important in determining the optical properties of tightly packed solid-state assemblies.[2d] We are currently investigating this direction with the design of nonconjugated dimers in which the interaction between dye subunits is modulated by linkers with tailored folding behavior. Arguably, curcuminoid-BF_2 do belong to a versatile class of organic dyes on which to base the generation of supramolecular systems endowed with visible to near-infrared fluorescence emission and photochemical properties for applications in sensing and photochromic materials.

Experimental Section

Materials. All solvents for synthesis were of analytic grade. Spectroscopy measurements were carried out with spectroscopic grade solvents. NMR spectra (^1H, ^{13}C) were recorded at room temperature on a JEOL JNM ECS 400 (400 and 100 MHz for ^1H and ^{13}C, respectively). Data are listed in parts per million (ppm) and are reported relative to tetramethylsilane (^1H); residual solvent peaks of the deuterated solvents were used as an internal standard. 2D COSY and ROESY spectra were obtained using a Bruker Avance 500 (500 MHz). High resolution mass spectra were realized in Spectropole de Marseille (http://www.spectropole.fr/).

UV-Vis-absorption spectra were measured on Varian Cary 50 and a dual-beam JASCO V-670 spectrophotometer. Photochemical experiments under monochromatic irradiation were carried out using a Xe arc lamp (1000 W) equipped with a OMNI 300 grating monochromator (LOT QuantumDesign).

Fluorescence emission spectra were uncorrected and measured on a Cary Eclipse Fluorescence Spectrophotometer.

Fluorescence decays were obtained by the time-correlated single-photon counting (TC-SPC) method using a femtosecond laser excitation composed of a Titanium-Sapphire laser (Tsunami, Spectra-Physics) pumped by a doubled Nd:YVO_4 laser (Millennia Xs, Spectra-Physics). Light pulses at 880 nm (960 nm) from the oscillator were selected by an acousto-optic crystal at a repetition rate of 4 MHz, and then doubled at 440 nm (480 nm) by a nonlinear crystal. Fluorescence photons were detected at 90° through a monochromator and a polarizer at magic angle by means of a Hamamatsu MCP-PMT R3809U photomultiplier, connected to a SPC-630 TCSPC module from Becker & Hickl. The fluorescence data were analyzed using Globals software package (Laboratory for Fluorescence Dynamics, University of Illinois at Urbana−Champaign).[23]

Electrochemistry. Cyclic voltammetry was performed using a BAS 100 Potentiostat (Bioanalytical Systems) and the data were analyzed with BAS100W soft-ware (v2.3). A Pt working electrode (diameter 1.6 mm), a Pt counter electrode and a Ag/AgCl (3 M NaCl solution) reference electrode were used. Cyclic voltammograms were recorded at a scan rate of 100 mV s^{-1} for solutions of the compounds (concentration *ca*. 10^{-3} M) in dichloromethane containing (*n*-Bu)$_4$NPF_6 (0.1 M) as supporting electrolyte. Ferrocene was used as an internal standard.

Computational details. Ground state geometry optimizations of curcumin dimers and photodimers were performed in the gas phase using density functional theory (DFT) with the ωB97X-D exchange-correlation functional[33] (XCF) and the 6-31+G(d) basis set. The use of a long-range dispersion-corrected XCF was employed in order to accurately describe weak interactions between the curcuminoid chromophores. Molecular structures were confirmed as real minima of the potential energy surface on the basis of their harmonic vibrational frequencies, which showed positive force constants for all normal modes.

Syntheses. For the synthesis of precursor compounds shown in Scheme 1 see the Supporting Information.

C12-Me

Hemicurcuminoid-BF_2 **5** (610 mg, 2.29 mmol) was dissolved in 10 mL of ethyl acetate and the solution was heated up to 60°C. 1,12-Bis(4-formylphenoxy)dodecane **2** (378 mg, 0.92 mmol) and tri-*n*-butylborate (500 µL, 1.84 mmol) were dissolved into 10 mL of ethyl acetate and the solution was added to the reaction mixture. After 30 min at 60°C, a first portion of *n*-butylamine (91 µL, 0.92 mmol) was added to the solution. A second portion of *n*-butylamine (91 µL, 0.92 mmol) was added after 2 h and the mixture was stirred overnight at 60 °C. After cooling, the precipitate was filtered off under vacuum. The solid was purified on a silica gel column with dichloromethane as an eluent, giving **C12-Me** as an orange powder (210 mg, 25 %). ^{1}H NMR (400 MHz, [D_6]DMSO): δ=7.98 (d, $^3J_{H\text{-}H}$=15.6 Hz, 4H, olefinic H), 7.85 (d, $^3J_{H\text{-}H}$=8.7 Hz, 4H, Ar-H), 7.83 (d, $^3J_{H\text{-}H}$=8.7 Hz, 4H, Ar-H), 7.06 (m, 12H, Ar-H, olefinic H), 6.50 (s, 2H, C-H *meso*), 4.06 (t, $^3J_{H\text{-}H}$=6.4 Hz, 4H, CH_2), 3.85 (s, 6H, CH_3), 1.77–1.68 (m, 4H, CH_2), 1.41–1.27 ppm (m, 16H, CH_2); HRMS (ESI): *m*/*z* calcd for $C_{52}H_{56}O_8F_4B_2Na^+$: 929.4007 $[M+Na]^+$; found: 929.4011.

C12-EH

Compound **3** (1.0 g, 1.49 mmol) was dissolved in 20 mL of toluene and stirred at reflux for 30 min under argon. 4-[(2-Ethylhexyl)oxy]-benzaldehyde **1** (872 mg, 3.72 mmol) and tri-*n*-butylborate (1.10 mL, 3.87 mmol) were dissolved into 70 mL of toluene and the solution was added dropwise into the reaction mixture. After stirring for 30 min at reflux, a first portion of *n*-butylamine (74 µL, 0.74 mmol) was added. After 2 h a second portion of *n*-butylamine (74 µL, 0.74 mmol) was added and the reaction mixture was stirred at reflux overnight. After cooling, the precipitate was filtered off under vacuum. The crude product was purified on a silica gel column with cyclohexane/dichloromethane (7/3 v:v) as eluent giving **C12-EH** as an orange powder (20 mg, 3%). ^{1}H NMR (400 MHz, CD_2Cl_2): δ=7.97 (d, $^3J_{H\text{-}H}$=15.5 Hz, 4H, olefinic H), 7.60 (d, $^3J_{H\text{-}H}$=8.8 Hz, 8H, Ar-H), 6.96 (d, $^3J_{H\text{-}H}$=8.8 Hz, 4H, Ar-H), 6.95 (d, $^3J_{H\text{-}H}$=8.8 Hz, 4H, Ar-H), 6.64 (d, $^3J_{H\text{-}H}$=15.5 Hz, 4H, olefinic H), 6.06 (s, 2H, C-H *meso*), 4.02 (t, $^3J_{H\text{-}H}$=6.6 Hz, 4H, CH_2), 3.92 (d, $^3J_{H\text{-}H}$=5.9 Hz, 4H, CH_2), 1.86–1.68 (m, 6H), 1.52–1.40 (m, 12H, CH_2), 1.39–1.28 (m, 20H, CH_2), 0.93 (t, $^3J_{H\text{-}H}$=7.5 Hz, 6H, CH_3), 0.91 ppm (t, $^3J_{H\text{-}H}$=7 Hz, 6H, CH_3); HRMS (ESI) *m*/*z* calcd for $C_{66}H_{84}O_8F_4B_2Na^+$: 1102.6201 $[M+Na]^+$; found: 1102.6204.

C6O4-Me

Hemicurcuminoid-BF_2 **5** (560 mg, 2.10 mmol) was dissolved in 10 mL of ethyl acetate and the solution was heated up to 60°C. 1,8-Bis[2-(4-formylphenoxy)ethoxy]ethane **4** (300 mg, 0.84 mmol) and tri-*n*-butylborate (450 µL, 1.68 mmol) were dissolved in 10 mL of ethyl acetate and the solution was added to the reaction mixture. After 30 min at 60°C, a first portion of *n*-

butylamine (80 µL, 0.84 mmol) was added to the solution. A second portion of *n*-butylamine (80 µL, 0.84 mmol) was added after 2 h and the mixture was stirred overnight at 60°C. After cooling, the precipitate was filtered off under vacuum. The solid was purified on silica gel column with dichloromethane as eluent, giving a product as a red powder (90 mg, 13 %). ^{1}H NMR (400 MHz, [D$_6$]DMSO): δ=7.97 (d, $^{3}J_{H\text{-}H}$=15.6 Hz, 2H, olefinic H), 7.96 (d, $^{3}J_{H\text{-}H}$=15.6 Hz, 2H, olefinic H), 7.83 (d, $^{3}J_{H\text{-}H}$=8.7 Hz, 4H, Ar-H), 7.82 (d, $^{3}J_{H\text{-}H}$=8.7 Hz, 4H, Ar-H), 7.06–7.02 (m, 12H, Ar-H, olefinic H), 6.48 (s, 2H, C-H *meso*), 4.24–4.14 (m, 4H, CH_2), 3.84 (s, 6H, CH_3), 3.80–3.74 (m, 4H, CH_2), 3.62 ppm (s, 4H, CH_2); ^{13}C NMR (100 MHz, $CDCl_3$): δ=179.2, 162.6, 161.8, 146.4, 131.8, 126.9, 118.7, 115.3, 114.9, 101.7, 70.0, 68.8, 67.5, 55.9 ppm; HRMS (ESI) *m*/*z* calcd for $C_{46}H_{44}O_{10}F_4B_2Na^+$: 877.2964 $[M+Na]^+$; found : 877.2963.

Acknowledgements

EZ and FF acknowledge Aix Marseille Université and CNRS for financial support. Dr R. Rosas (Spectropole Marseille) is acknowledged for her help in obtaining 2D COSY and ROESY spectra. OU and DC thank MINECO/FEDER of the Spanish Government for financial support (project CTQ2016-80955-P). This work was also supported by the Transnational Laboratory QuantumChemPhys (ANR-10-IDEX-03-02), established between the University of Bordeaux, Euskal Herriko Unibertsitatea and Donostia International Physics Center.

Conflict of interest

The authors declare no conflict of interests

Keywords: dyes/pigments, excimer, excitonic coupling, foldamers, fluorescence, photochemistry

[1] a) See for example: U. H. F. Bunz, J. Freudenberg, *Acc. Chem. Res*. **2019**, *52*, 1575; b) J. Hou, O. Inganäs, R. H. Friend, F. Gao, *Nat. Mater.* **2017**, *17*, 119; c) A. J. C. Kuehne, M. C. Gather, *Chem. Rev*. **2016**, *116*, 12823; d) A. Mishra, P. Bäuerle, *Angew. Chem. Int. Ed*. **2012**, *51*, 2020; e) Y. Tao, K. Yuan, T. Chen, P. Xu, H. Li, R. Chen, C. Zheng, L. Zhang, W. Huang, *Adv. Mater.* **2014**, *26*, 7931; f) B. C. Thompson, J. M. J. Fréchet, *Angew. Chem. Int. Ed*. **2008**, 47*,* 58; g) C. Lee, S. Lee, G.-U Kim, W. Lee, B. J. Kim, *Chem. Rev*. **2019**, *119*, 8028; h) J. Urieta-Mora, I. García-Benito, A. Molina-Ontoria, N. Martín, *Chem. Soc. Rev*. **2018**, *47*, 8541; i) C. Zhang, P. Chen, W. Hu, *Small* **2016**, *12*, 1252; j)

G. Qian, Z. Y. Wang, *Chem. Asian J*. **2010**, *5*, 1006; j) H. Jia, T. Lei, *J. Mater. Chem. C* **2019**, *7*, 12809.

[2] a) S. M. Menke, R. J. Holmes, *Energy Environ. Sci*. **2014**, *7*, 499; b) P. M. Beaujuge, J. M. J. Fréchet, *J. Am. Chem. Soc*. **2011**, *133*, 20009; c) J. Liu, H. Zhang, H. Dong, L. Meng, L. Jiang, L. Jiang, Y. Wang, J. Yu, Y. Sun, W. Hu, A. J. Heeger, *Nat. Commun*. **2015**, *6*, 10032; d) N. J. Hestand, N. C. Spano, *Chem. Rev*. **2018**, *118*, 7069; e) J. L. Banal, B. Zhang, D. J. Jones, K. P. Ghiggino, W. W. H. Wong, *Acc. Chem. Res.* **2017**, *50*, 49; f) K. H. Park, W. Kim, J. Yang, D. Kim, *Chem. Soc. Rev*. **2018**, *47*, 4279; g) J. Cornil, D. Beljonne, J.-P. Calbert, J.-L. Brédas, *Adv. Mater.* **2001**, *13*, 1053.

[3] a) G. Chen, H. Sasabe, T. Igarashi, Z. Hong, J. Kido, *J. Mater. Chem. A* **2015**, *3*, 14517; b) J. Daniel, A. G. Godin, M. Palayret, B. Lounis, L. Cognet, M. Blanchard-Desce, J. *Phys. D: Appl. Phys.* **2016**, *49*, 084002; c) O. Mongin, L. Porrès, M. Charlot, C. Katan, M. Blanchard-Desce, *Chem. – Eur. J*. **2007**, *13*, 1481; d) H. Y. Woo, B. Liu, B. Kohler, D. Korystov, A. Mikhailovsky, G. C. Bazan, *J. Am. Chem. Soc*. **2005**, *127*, 14721; e) M. Montalti, L. Prodi, E. Rampazzo, N. Zaccheroni, *Chem. Soc. Rev*. **2014**, *43*, 4243; f) W. Ni, X. Wan, M. Li, Y. Wang, Y. Chen, *Chem. Commun*. **2015**, *51*, 4936; g) B. Dereka, A. Rosspeintner, Z. Li, R. Liska, E. Vauthey, *J. Am. Chem. Soc*. **2016**, *138*, 4643; h) F. B. Dias, K. N. Bourdakos, V. Jankus, K. C. Moss, K. T. Kamtekar, V. Bhalla, J. Santos, M. R. Bryce, A. P. Monkman, *Adv. Mater*. **2013**, *25*, 3707.

[4] a) G. D'Avino, F. Terenziani, A. Painelli, *J. Phys. Chem. B* **2006** *110*, 25590; b) S. Sanyal, A. Painelli, S. K. Pati, F. Terenziani, C. Sissa, *Phys. Chem. Chem. Phys.* **2016**, *18*, 28198; c) C. Zheng, C. Zhong, C. J. Collison, F. C. Spano, *J. Phys. Chem. C* **2019**, *123*, 3203; d) X.-K. Chen, D. Kim, J.-L. Brédas, *Acc. Chem. Res*. **2018**, *51*, 2215.

[5] A. D'Aléo, A. Felouat, V. Heresanu, A. Ranguis, D. Chaudanson, A. Karapetyan, M. Giorgi, F. Fages, *J. Mater. Chem. C* **2014**, *2*, 5208.

[6] G. M. Day, *Crystallogr. Rev*. **2011**, *17*, 3.

[7] a) A. Zitzler-Kunkel, E. Kirchner, D. Bialas, C. Simon, F. Würthner, *Chem.–Eur. J*. **2015**, *21*, 14851;b) D. Bialas, C. Zhong, F. Würthner, F. C. Spano, *J. Phys. Chem. C* **2019**, *123*, 18654; c) D. Bialas, A. Zitzler-Kunkel, E. Kirchner, D. Schmidt, F. Würthner, *Nat. Commun*. **2016**, 7*,* 12949; d) F. Würthner, *Acc. Chem. Res*. **2016**, *49*, 868; e) E. Kirchner, D. Bialas, F. Fennel, M. Grüne, F. Würthner, *J. Am. Chem. Soc.* **2019**, *141*, 7428. f) E. Kirchner, D. Bialas, M. Wehner, D. Schmidt, F. Würthner, *Chem.–Eur. J.* **2019**, *25*, 11285.

[8] D. Li, W. Hu, J. Wang, Q. Zhang, X.-M. Cao, X. Ma, H. Tian, *Chem. Sci*. **2018**, *9*, 5709.

[9] F. C. De Schryver, P. Collart, J. Vandendriessche, R. Goedeweeck, A. M. Swinnen, M. Van der Auweraer, *Acc. Chem. Res*. **1987**, *20*, 159.

[10] H. Bouas-Laurent, Alain Castellan, J.-P. Desvergne, *Pure Appl. Chem*. **1980**, *52*, 2633.

[11] J.-P. Desvergne, H. Bouas-Laurent, R. Sarrebeyroux, *Isr. J. Chem*. **1979**, *18*, 220.

[12] a) L. Lu, R. J. Lachicotte, T. L. Penner, J. Perlstein, D. G. Whitten, *J. Am. Chem. Soc*. **1999**, *121*, 8146; b) L. J. Patalag, L. P. Ho, P. G. Jones, D. B. Werz, *J. Am. Chem. Soc*. **2017**, *139*, 15104; c) Y. Sasano, R. Sato, Y. Shigeta, N. Yasuda, H. Maeda, *J. Org. Chem*. **2017**, *82*, 11166;

[13] a) K. Liang, M. S. Farahat, J. Perlstein, K.-Y. Law, D. G. Whitten, *J. Am. Chem. Soc.* **1997**, *119*, 830; b) I. A. Karpenko, M. Collot, L. Richert, C. Valencia, P. Villa, Y. Mély, M. Hibert, D. Bonnet, A. S. Klymchenko, *J. Am. Chem. Soc*. **2015**, *137*, 405; c) C. Sissa, F. Terenziani, A. Painelli, A. Abbotto, L. Bellotto, C. Marinzi, E. Garbin, C. Ferrante, R. Bozio, *J. Phys. Chem*. B **2010**, *114*, 882.

[14] O. Uranga-Barandiaran, M. Catherin, E. Zaborova, A. D'Aléo, F. Fages, F. Castet, D. Casanova, *Phys. Chem. Chem. Phys*. **2018**, *20*, 24623.

[15] A. Felouat, A. D'Aléo, F. Fages, *J. Org. Chem*. **2013**, *78*, 4446.

[16] a) D.-H. Kim, A. D'Aléo, X.-K. Chen, A. D. S. Sandanayaka, D. Yao, L. Zhao, T. Komino, E. Zaborova, G. Canard, Y. Tsuchiya, E. Choi, J. W. Wu, F. Fages, J.-L. Brédas, J.-C. Ribierre, C. Adachi, *Nat. Photonics* **2018**, *12*, 98; b) H. Ye, D. H. Kim, X. Chen, A. S. D. Sandanayaka, J. U. Kim, E. Zaborova, G. Canard, Y. Tsuchiya, E. Choi, J. W. Wu, F. Fages, J.-L. Brédas, A. D'Aléo, J.-C. Ribierre, C. Adachi, *Chem. Mater*. **2018**, *30*, 6702.

[17] K. Kamada, T. Namikawa, S. Senatore, C. Matthews, P.-F. Lenne, O. Maury, C. Andraud, M. Ponce-Vargas, B. Le Guennic, D. Jacquemin, P. Agbo, D. D. An, S. S. Gauny, X. Liu, R. J. Abergel, F. Fages, A. D'Aléo, *Chem.–Eur. J.* **2016**, *22*, 5219.

[18] F. Archet, D. Yao, S. Chambon, M. Abbas, A. D'Aléo, G. Canard, M. Ponce-Vargas, E. Zaborova, B. Le Guennic, G. Wantz, F. Fages, *ACS Energy Lett*. **2017**, *2*, 1303.

[19] a) V. Polishchuk, M. Stanko, A. Kulinich, M. Shandura, *Eur. J. Org. Chem*. **2018**, 240; b) Y. Li, J. Yang, H. Liu, J. Yang, L. Du, H. Feng, Y. Tian, J. Cao, C. Ran, *Chem. Sci*. **2017**, *8*, 7710; c) G. Bai, C. Yu, C. Cheng, E. Hao, Y. Wei, X. Mu, L. Jiao, *Org. Biomol. Chem*. **2014**, *12*, 1618; d) L. Zhai, M. Liu, P. Xue, J. Sun, P. Gong, Z. Zhang, J. Sun, R. Lu, *J. Mater. Chem. C* **2016**, *4*, 7939.

[20] I. J. Olavarría-Contreras, A. Etcheverry-Berríos,W. Qian, C. Gutíerrez-Cerón, A. Campos-Olguín, E. C. Sañudo, D. Dulic, E. Ruiz, N. Aliaga-Alcalde, M. Soler, H. S. J. van der Zant, *Chem. Sci*. **2018**, *9*, 6988.

[21] S. Bellinger, M. Hatamimoslehabadi, R. E. Borg, J. La, P. Catsoulis, F. Mithila, C. Yelleswarapu, J. Rochford, *Chem. Commun*. **2018**, *54*, 6352.

[22] G. Canard, M. Ponce-Vargas, D. Jacquemin, B. Le Guennic, A. Felouat, M. Rivoal, E. Zaborova, A. D'Aléo, F. Fages, *RSC Adv*. **2017**, *7*, 10132.

[23] M. Louis, A. Brosseau, R. Guillot, F. Ito, C. Allain, R. Métivier, *J. Phys. Chem. C* **2017**, *121*, 15897.

[24] E. Kim, A. Felouat, E. Zaborova, J.-C. Ribierre, J. W. Wu, S. Senatore, C. Matthews, P.-F. Lenne, C. Baffert, A. Karapetyan, M. Giorgi, D. Jacquemin, M. Ponce-Vargas, B. Le Guennic, F. Fages, A. D'Aléo, *Org. Biomol. Chem*. **2016**,*14*, 1311.

[25] a) T. B. Nguyen, A. Al-Mourabit, Photochem. Photobio. Sci. 2016, 15, 1115; b) G. Montaudo, S. Caccamese, V. Librando, *Org. Magn. Reson*. **1974**, *6*, 534.

[26] a) G. M. J. Schmidt, *J. Chem. Soc*. **1964**, 2014; b) S. d'Agostino, F. Spinelli, E. Boanini, D. Braga, F. Grepioni, *Chem. Commun*. **2016**, *52*, 1899; c) S. Kodama, K. Johmoto, A. Sekine, K. Fujii, H. Uekusa, *CrystEngComm* **2013**, *15*, 4667.

[27] H. Tadokoro, Y. Chatani, Y. Yoshihara, S. Tahara, S. Murahashi, *Makromol. Chem*. **1964**, *73*, 109.

[28] F. C. Spano, *Acc. Chem. Res*. **2010**, *43*, 429.

[29] F. C. Spano, *J. Am. Chem. Soc*. **2009**, *131*, 4267.

[30] P. Reynders, H. Dreeskamp, W. Kühnle, K. A. Zachariasse, *J. Phys. Chem*. **1987**, *91*, 3982.

[31] C. Kaufmann, W. Kim, A. Nowak-Król, Y. Hong, D. Kim, F. Würthner, *J. Am. Chem. Soc*. **2018**, *140*, 4253.

[32] J. B. Birks, *Photophysics of Aromatic Molecules*, Wiley, New York, **1970**.

[33] J.-D. Chai, M. Head-Gordon, *Phys. Chem. Chem. Phys*. **2008**, *10*, 6615.

Entry for the Table of Contents

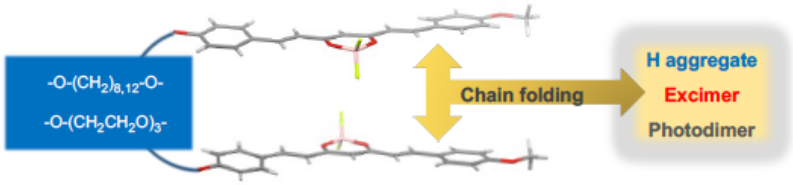

A series of covalently-linked dimers of quadrupolar curcuminoid-BF_2 dyes has been synthesized. They display solvent-dependent UV/Vis absorption and fluorescence emission as a result of a folding process controlling intramolecular chromophore aggregation. An in-depth investigation of their photophysical properties allowed establishing a complex kinetic scheme and provided a rationale for the formation of the first example of photodimerization of the curcuminoid chromophore.